Along-strike variations in the shallow seismic velocity structure of the Seattle fault zone: Evidence for fault segmentation beneath Puget Sound

Andrew J. Calvert
Department of Earth Sciences, Simon Fraser University, Burnaby, British Columbia, Canada

Michael A. Fisher
U.S. Geological Survey, Menlo Park, California, USA

Samuel Y. Johnson
U.S. Geological Survey, Denver, Colorado, USA

SHIPS Working Group[1]

Received 6 December 2001; revised 1 June 2002; accepted 9 August 2002; published 3 January 2003.

[1] Around 1100 years ago, the Seattle fault, which trends east-west beneath Puget Sound and the greater Seattle metropolitan area, experienced a $M > 7$ earthquake. We present high-resolution images of the shallow P wave velocity variation across the fault zone. These images were obtained by tomographic inversion of the first arrivals recorded along two north-south oriented seismic reflection lines shot within Puget Sound near Seattle. Just beneath the seafloor, the fault zone includes uplifted Tertiary rocks with seismic velocities in the range of 2300 to 2600 m s^{-1}. These velocities contrast markedly with values of $\sim$1600 m s^{-1} in shallow Holocene sediments. South of the Seattle fault zone volcanic rocks of the Crescent Formation, which exhibit velocities >3700 m s^{-1}, are identified at depths of only 900 m. Seismic velocities of around 2600 m s^{-1}, which represent Oligocene rocks, are found in the hanging wall of the Seattle fault beneath eastern Puget Sound. In the west, lower, 2300 m s^{-1} seismic velocities occur, probably due to the presence of Miocene rocks, which are not found in the east. Along-strike velocity variations arise from the folding of Tertiary rocks and the presence of distinct fault splays, including a north striking tear fault characterized by depressed seismic velocities that was intersected by the eastern seismic line. Along-strike differences in the uplift of Tertiary rocks beneath Puget Sound are likely associated with the existence of a segment boundary of the Seattle fault system. *INDEX TERMS:* 7205 Seismology: Continental crust (1242); 7223 Seismology: Seismic hazard assessment and prediction; 7230 Seismology: Seismicity and seismotectonics; 8107 Tectonophysics: Continental neotectonics; 8180 Tectonophysics: Evolution of the Earth: Tomography; *KEYWORDS:* Seattle Fault, seismic reflection, first arrival tomography, seismic velocity, seismic hazard

Citation: Calvert, A. J., M. A. Fisher, S. Y. Johnson, and SHIPS Working Group, Along-strike variations in the shallow seismic velocity structure of the Seattle fault zone: Evidence for fault segmentation beneath Puget Sound, *J. Geophys. Res.*, *108*(B1), 2005, doi:10.1029/2001JB001703, 2003.

1. Introduction

[2] The Puget Lowland of western Washington is a forearc basin located between the Cascade volcanic arc in the east and the Olympic mountains on the west, which form part of the accretionary complex of the Cascadia subduction zone. Eocene volcanic rocks of the Crescent Formation, which are exposed in the Olympic mountains and extend beneath the western part of the Puget Lowland, are in thrust faulted contact with the accreted sediments. Detailed mapping of the bedrock geology across the Puget Lowland has been hampered by the extensive Quaternary sedimentary cover; however, industry boreholes as deep as 3500 m, seismic

[1]The SHIPS Working Group includes T. M. Brocher, U.S. Geological Survey; K. C. Creager, Department of Earth and Space Sciences, University of Washington; R. S. Crosson, Department of Earth and Space Sciences, University of Washington; R. D. Hyndman, Geological Survey of Canada; K. C. Miller, Department of Geological Sciences, University of Texas at El Paso; D. Mosher, Geological Survey of Canada; T. Parsons, U.S. Geological Survey; T. L. Pratt, U.S. Geological Survey; G. Spence, School of Earth and Ocean Sciences, University of Victoria, Canada; U. ten Brink, U.S. Geological Survey; A. M. Trehu, College of Oceanic and Atmospheric Sciences, Oregon State University; and C. S. Weaver, U.S. Geological Survey.

0148-0227/03/2001JB001703$09.00

reflection surveys and potential field data in combination with the scarce pre-Quaternary outcrops have been used to delineate the major upper crustal structures. The Tacoma, Seattle, and Everett sedimentary basins are apparent in Bouguer gravity anomaly maps; they form a sequence of distinct lows trending north-northeast through the Puget Lowland [*Finn et al.*, 1991]. The Tacoma basin is 4 km deep and underlain by Crescent volcanics, which are exposed to the south. The Tacoma and Seattle basins are separated by a region of uplifted and folded rocks termed the Seattle uplift, in which Crescent volcanic rocks occur at <1 km depth [*Pratt et al.*, 1997]. The boundary between the Seattle uplift and the ~9-km-deep Seattle basin is marked by steeply north dipping strata that are deformed and cut by faults of the Seattle fault zone. The depth of the Seattle basin decreases to the north, where it onlaps the Kingston arch, a broad anticline of folded strata that can be identified in seismic reflection profiles [*Johnson et al.*, 1994; *Pratt et al.*, 1997].

[3] Although numerous earthquakes are recorded each year beneath the Puget Lowland, those events with magnitude >6 are deep, and associated with the subducting Juan de Fuca slab. No crustal earthquakes with magnitude >6 have been instrumentally recorded west of the Cascade range [*Ludwin et al.*, 1991]. Nevertheless, recent geological mapping of offsets in Quaternary strata and tsunami deposits has documented evidence of large prehistoric crustal earthquakes [*Gower et al.*, 1985; *Atwater and Moore*, 1992; *Bourgeois and Johnson*, 2001]. In particular, 7 m of uplift along part of the Seattle fault suggests that an earthquake with magnitude >7 occurred around 1100 years ago [*Bucknam et al.*, 1992]. The realization that crustal earthquakes in the Puget Lowland represent a major seismic hazard has motivated a number of recent seismic reflection studies, including this one, aimed at mapping subsurface structures, and the Seattle fault zone in particular since it cuts through greater Seattle and other densely populated areas [*Johnson et al.*, 1994; *Johnson et al.*, 1999].

[4] In 1998, the Seismic Hazards Investigation in Puget Sound (SHIPS) program acquired seismic reflection data through Puget Sound as part of a larger wide-angle and multichannel reflection survey aimed at mapping the subsurface architecture and relating it to mapped surface structures [*Fisher et al.*, 1999]. The SHIPS program is a collaborative project between the United States Geological Survey, the Geological Survey of Canada, and a number of U.S. and Canadian universities. In this paper, we analyze the travel times of first arrivals, which include direct water waves, refractions, diving waves, and diffractions recorded in two single-ship reflection lines across the Seattle fault zone. Preliminary first arrival tomography results from the crossing of the fault zone by SHIPS line PS-2 were reported by *Calvert et al.* [2001]. We present here more refined high-resolution *P* wave velocity images of the fault zone that were generated by tomographic inversion of travel times recorded along SHIPS seismic lines PS-1 and PS-2, which cross the fault zone in Puget Sound close to downtown Seattle (Figure 1).

[5] Bedrock velocities have been determined across terrane boundaries using first arrivals recorded in deep seismic reflection profiles on Vancouver Island by a conventional statics analysis [*Mayrand et al.*, 1987], and in Alaska by iterative forward modeling [*Brocher et al.*, 1989]. More recently, relatively precise mapping of lateral velocity variations in the near-surface has become possible with the advent of various tomographic inversion methods. Such techniques have occasionally been applied to first arrivals recorded in deep reflection surveys shot on land [*Brocher et al.*, 1991; *Schmid et al.*, 2001], although the results have sometimes been degraded by crooked acquisition profiles. In a shallow investigation, first arrival tomography was used to infer faulting in the upper 100 m from velocity variations in unconsolidated sediments near the epicenter of the Northridge earthquake in California [*Catchings et al.*, 1998]. Yet first arrival analysis and its integration with reflection data in a unified interpretation of the near-surface geology is essentially nonexistent offshore, despite the fact that a number of seismogenic faults are readily accessible to marine surveys. In fact in many urban areas, marine surveys are the only practical way of acquiring seismic data due to limitations on access, and the waterways around the city of Seattle provide an excellent example of this situation. This paper represents an integration of velocity images from the two SHIPS crossings of the Seattle fault zone with existing geological and geophysical data; the velocity images provide an essential link between the surface geology and the subsurface seismic reflectors. Our results show that high-resolution first arrival tomography is an important new tool for determining structure in areas of complex geology where seismic reflectors are absent due to steep or overturned dips. The two velocity models that we have derived clearly show major along-strike variations within the Seattle fault zone in both the number of fault splays and the degree of uplift of Tertiary lithologies over a distance of <3 km. We interpret this as implying the existence of a segment boundary in the Seattle fault beneath Puget Sound.

2. Seattle Fault and Basin Stratigraphy

[6] The Seattle fault zone strikes east-west beneath the Puget Lowland, and separates the ~9-km-deep Seattle basin from the Seattle uplift to the south [*Johnson et al.*, 1994; *Blakely et al.*, 2002]. The Seattle fault was first inferred from gravity data in 1965, and the fault zone was interpreted to comprise two steeply north dipping normal faults with ~11 km of vertical displacement [*Danes et al.*, 1965]. Subsequent geological mapping [*Gower et al.*, 1985] led to the suggestion that the fault is a south dipping thrust [*Yount and Holmes*, 1992]. The Seattle fault is interpreted to transfer dextral motion from north striking faults in the Cascade foothills to other hypothesized north-south faults west of the Puget Lowland [*Johnson et al.*, 1994]. The Seattle fault accommodates some of the north-south shortening in the Puget Lowland recorded by geodetic data [*Khazaradze et al.*, 1999; *Miller et al.*, 2001], which is forced by oblique convergence along the Cascadia continental margin (Figure 1) [*Wells et al.*, 1998].

[7] Analysis of oil industry seismic reflection data indicates that the Seattle fault is a broad zone of deformation containing a number of south dipping reverse faults [*Johnson et al.*, 1994; *Pratt et al.*, 1997]. High-resolution marine seismic reflection surveys in Puget Sound and Lake Washington locate the Seattle fault zone at several points along its length, and reveal three to five fault splays [*Johnson et al.*, 1999]. The absence of clear reflections from either the fault planes or any stratigraphy within the fault zone makes

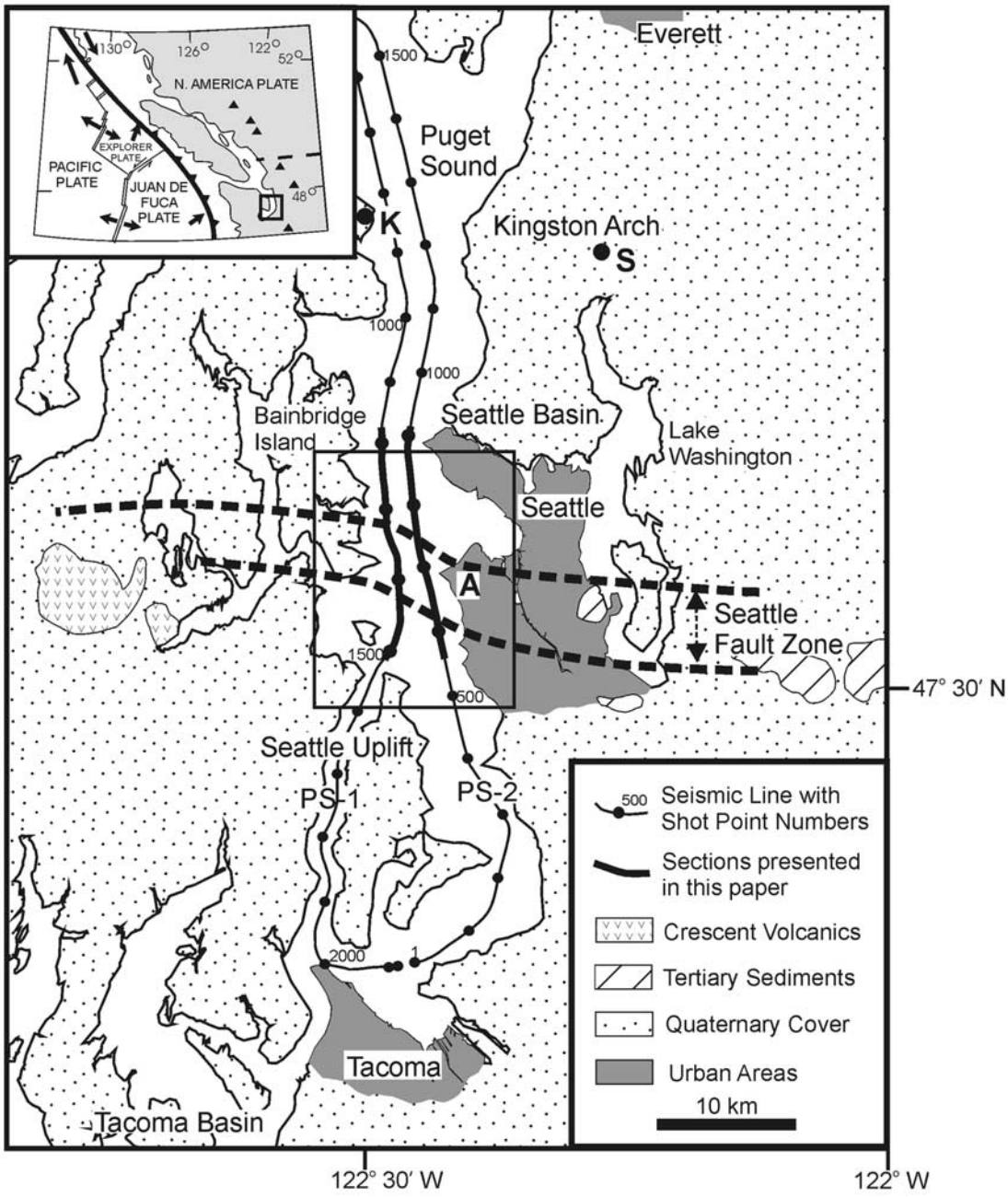

Figure 1. SHIPS seismic reflection profiles PS-1 and PS-2 superimposed on the geology of the Puget Lowland. The position of the survey area with respect to the Cascadia convergent margin is shown by the rectangle in the inset location map. Dots indicate every hundredth shot point along the seismic lines. The thicker lines correspond to the seismic data presented in this paper. A is Alki Point. K and S denote the locations of the Kingston 1 and Socal-Schroder 1 wells where sonic log data are available. The rectangle is the area shown in Figure 7.

unambiguous interpretation of the reflection data difficult. Thus the dips of the faults are uncertain. Dips as large as 70° have been proposed for one splay on the basis of coseismic offset patterns [*Bucknam et al.*, 1992]; on the basis of seismic reflection surveys a dip of between 45° and 60° has been inferred for the Seattle fault above 4 km depth [*Johnson et al.*, 1994, 1999]; dips as low as 20° have been suggested for the fault at greater depths [*Pratt et al.*, 1997]. Slip rates, which lie in the range 0.5–0.9 mm yr^{-1}, have been estimated at various locations along the Seattle fault zone [*Johnson et al.*, 1999; *Calvert et al.*, 2001].

[8] Interpretations of oil industry seismic sections and borehole data show that the Seattle basin is asymmetric in north-south cross section, reaching a depth of ~9 km close to the Seattle fault beneath Puget Sound, and is floored by volcanics of the Eocene Crescent Formation [*Johnson et al.*, 1994; *Pratt et al.*, 1997; *Brocher et al.*, 2001]. The Crescent Formation was penetrated by an exploration well in the area

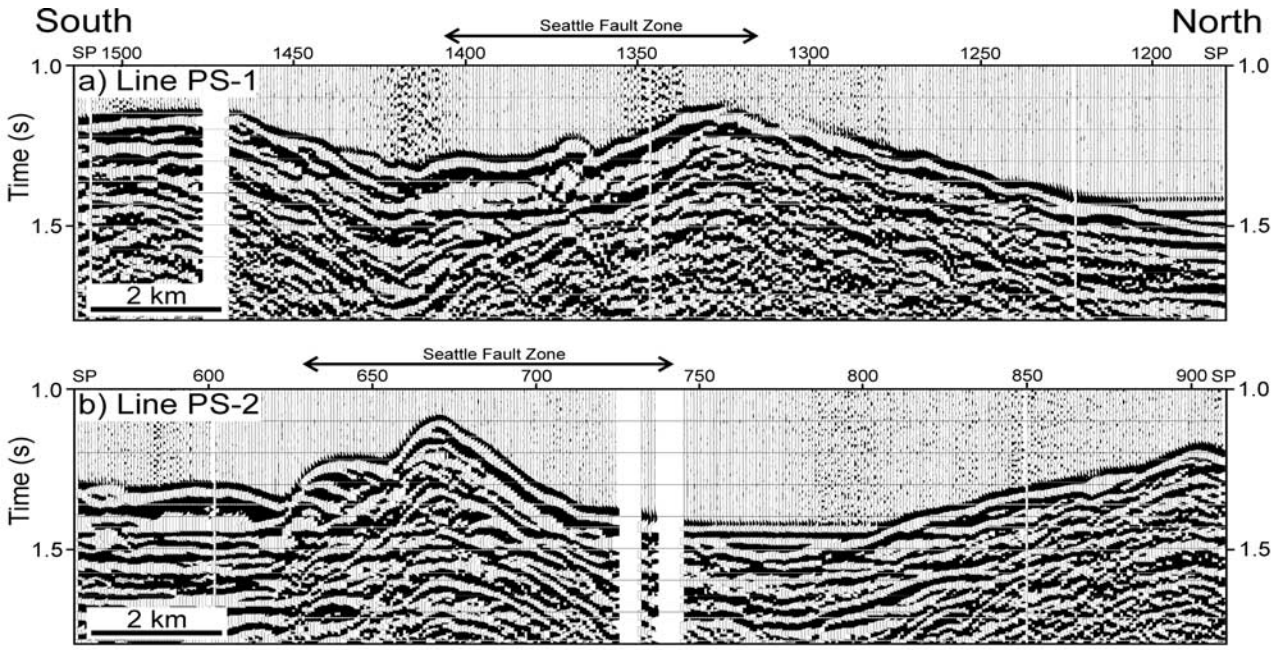

Figure 2. Unfiltered common offset gathers from (a) line PS-1 and (b) line PS-2 across the Seattle fault zone. The source-receiver offset is 2100 m. First arrivals can be identified as the first strong arrivals on the section. High-velocity rocks close to the seafloor within the fault zone cause arrivals to be locally early, at around 1.1 s. Shot point values corresponding to the common midpoint locations of the seismic traces are annotated.

of the Kingston arch, on the northern edge of the Seattle basin. The upper part of the terrane comprises interbedded marine basalt and sedimentary rocks. In the deepest part of the basin, the Crescent Formation is overlain by ~1900 m of mainly mid-Eocene sediments, 3700 m of the late Eocene and Oligocene marine Blakeley Formation, 3000 m of the Miocene nonmarine Blakely Harbor Formation, and up to 1000 m of Quaternary sediments [*Johnson et al.*, 1994]. Seismic reflection data show that the shallowest Tertiary rocks are characterized by high-amplitude subparallel reflections, which are separated from the lower-amplitude, discontinuous hummocky reflections of the overlying Quaternary units by either a disconformity or, where the Tertiary units are folded, an angular unconformity. On seismic reflection sections, Quaternary sediments can be divided into two distinct seismic units: the lower is internally complex and corresponds to Pleistocene glacial and interglacial deposits; the upper unit comprises variable-amplitude, horizontal reflections and represents postglacial strata that have accumulated in remnant Pleistocene basins during the latest Pleistocene and Holocene [*Johnson et al.*, 1994]. These previous correlations of specific geologic units with seismic reflection character provide the detailed framework that allows us to identify many of the structures we observe in the SHIPS reflection lines.

3. Seismic Data

[9] Two SHIPS seismic reflection lines were shot north-south in Puget Sound; the western line is PS-1, and line PS-2 is in the east, close to the city of Seattle. The source was a 13-gun tuned air gun array with a total volume of 79 L (4838 cubic inches), and data were recorded by a 96-channel hydrophone streamer with 25 m group interval and 2575 m far offset. The 50 m shot point (SP) interval yielded a nominal 24-fold stacked reflection section; the fold is lower at times <1.0 s due to muting of shallow refraction arrivals. Although elevated levels of environmental noise can be locally observed, the seismic data are of good quality as indicated by the constant-offset sections from the hydrophone group located at 2100 m from the source (Figure 2). Skipped shots, most of which were caused by restrictions on shooting close to marine mammals, are represented by gaps in the constant offset section. First arrivals recorded over the Seattle fault zone are earlier than in adjacent areas due to the presence of shallow high-velocity rocks.

[10] The seismic data were edited to remove noisy recording channels and bad shot gathers. The travel times of first arrivals were picked on every remaining shot using an automated neural-network first-break picking algorithm; the algorithm was trained to pick the initial peak of the source signature. The quality of the automated picking was sometimes poor, particularly in noise-contaminated areas. Therefore the seismic data were first sorted into constant offset gathers, where trace-to-trace correlations of first arrivals are easier to discern, and the automated picks were manually corrected. The data were then resorted to shot gathers for final quality control of the manually edited picks. Travel time picks, which were made on the wavelet peak, were shifted earlier by 16 ms, an average value estimated from the entire set of first arrivals, to align them with the onset of seismic energy at the receiver. These first arrival times, which are typically estimated to be accurate to

within ±8 ms were then input to a two-dimensional (2-D) tomographic inversion algorithm. Approximately 1820 picks were available per kilometer of seismic line.

[11] The nonlinear tomography problem of inverting recorded travel times for a subsurface velocity model can be linearized and solved iteratively. The iterative procedure requires the tracing of rays from source to receiver, which can be both time consuming and subject to errors arising from shadow zones and multipaths. To avoid these problems, we used a tomographic inversion algorithm based on a finite difference solution to the eikonal equation, which provides first arrival travel times to all points of a 2-D subsurface velocity grid [*Aldridge and Oldenburg*, 1993]. Ray paths from each receiver back to the source are generated by following the steepest descent direction through the computed 2-D travel time field; this approach produces first arrival ray paths irrespective of wave type. At each iteration, a perturbation to the velocity model is obtained from the difference between the calculated and observed first arrival times. An initial model is required for the iterative inversion, and a simple 1-D velocity model was used below the laterally varying seafloor. The effect of different values of the subseafloor velocity gradient on the RMS error was estimated from a few trial inversions, and the gradient that gave the lowest error was chosen for the starting model. In the initial model, the subseafloor velocity increased with a gradient of 2.0 s^{-1} to 3500 m s^{-1}, at which point the gradient was reduced to 0.1 s^{-1} to prevent the inclusion of anomalously large velocities in the model. Velocities above the seafloor, which varied between 15 m and 230 m depth, were set to a constant value of 1488 m s^{-1} (Figures 3a and 3b), a value which was estimated from the direct water wave. For inversion of this marine data set, where the velocity in the water layer is relatively well known, we have modified the tomography algorithm to keep the velocity grid values in the water layer at the constant predefined value of 1488 m s^{-1}. The water depth was estimated from the seabed reflection time on the near-offset hydrophone group. The vertical and horizontal spacing of the velocity grid was 25 m. Regularizing constraints based on the second spatial derivatives (horizontal and vertical) of the model slownesses were employed in the inversion procedure. Additionally, a 75 m × 75 m convolutional smoothing operator was applied to the updated slowness model between iterations to prevent the introduction of any short wavelength variations. 18 iterations were computed, which reduced the root-mean-square (RMS) travel time residual from 79.4 ms to 6.8 ms for line PS-1 and from 168.4 ms to 8.7 ms for line PS-2.

[12] The value of the RMS travel time residual for an entire line gives no indication of the existence of large residuals at certain sections of the profile. Plots of the travel time residuals for each individual shot-receiver pair are shown in Figure 4; values are generally <10 ms. Large clusters of travel time residuals with magnitude >25 ms are only found between shots 1310 to 1340 on line PS-1. These values are associated with low amplitude first arrivals, some of which can be seen between SP 1300 and 1325 on the constant offset section shown in Figure 2. Vertical and horizontal bands with zero error correspond to skipped shot points and killed receiver groups, respectively. Slightly elevated travel time residuals of 10–15 ms are associated with specific subsurface locations, which appear in Figure 4 as diagonal striping, and the crossover point from the direct water wave to the seafloor refraction. The seafloor refraction occurs only on the most distant receivers channels, i.e., those with large numbers, where the thickness of the water layer is large and the subseafloor velocities are low, e.g., SP 1170 to 1250 on line PS-1 and SP 750 to 850 on line PS-2. Detailed examination of the travel time residuals indicates that, with the exception of the one region of line PS-1 discussed above, all observed travel times are reproduced well by the final velocity models.

4. Velocity Models

[13] In this section, we describe the main characteristics of the two velocity models derived by tomographic inversion of the first arrivals. A more complete interpretation is then presented in section 5, where a detailed correlation of the velocity models with the coincident reflection images is made.

4.1. Lithology and Faulting

[14] Away from the Seattle fault zone, the derived subseafloor *P* wave velocity models reveal an undulating high-velocity unit, in which the velocity increases with depth, that is overlain by a more uniform low-velocity fill (Figures 3c and 3d). The contact between these two units corresponds approximately to the 1800 m s^{-1} isovelocity contour. Our inversion shows that velocities in the upper unit range from 1500 to 1800 m s^{-1}, and we interpret this unit to be unconsolidated postglacial Quaternary deposits because these strata fill small basins in the underlying higher velocity strata. In the underlying unit, velocities increase gradually from 1800 to 2200–2400 m s^{-1} and then jump more sharply to around 3000 m s^{-1} over a 300 m depth range. *Brocher and Ruebel* [1998] report that the average sonic velocities for Pleistocene units in the Kingston 1 and Socal-Schroeder 1 wells, which lie 30 km from the Seattle fault zone (Figure 1), are 1830 and 1590 m s^{-1}, respectively; however, velocities as high as 2050 m s^{-1} are found at the base of the Pleistocene glacial deposits in the Kingston 1 well. Onshore seismic refraction surveys measured interval velocities as high as 2090 m s^{-1} and 2395 m s^{-1} in Pleistocene strata within 40 m of the surface [*Williams et al.*, 1999]. We therefore interpret the upper part of the unit that underlies the postglacial strata, where velocities are <2200–2400 m s^{-1}, to be glacial Pleistocene deposits, and we identify the lower part, in which velocities increase to around 3000 m s^{-1} to be the upper part of the Tertiary sedimentary section. Unusually high velocities, >3700 m s^{-1}, occur at 800–1000 m depth at the southern end of lines PS-1 and PS-2. These velocities are interpreted to represent volcanic rocks of the Crescent Formation, because such rocks are characterized in sonic logs by velocities of 4000–5000 m s^{-1} [*Brocher and Ruebel*, 1998].

[15] The velocity model along line PS-2 shows that the Seattle fault zone beneath eastern Puget Sound includes a single 2.5-km-wide region of uplifted, high-velocity, Tertiary rocks. Rocks with velocities of 2000 m s^{-1} are exposed at the seafloor, and the uplift zone is cored by rocks just 170 m below the seafloor with velocities as high as 2600 m s^{-1}. The high-velocity rocks within the uplifted block are restricted to a narrow zone that is 700 m wide

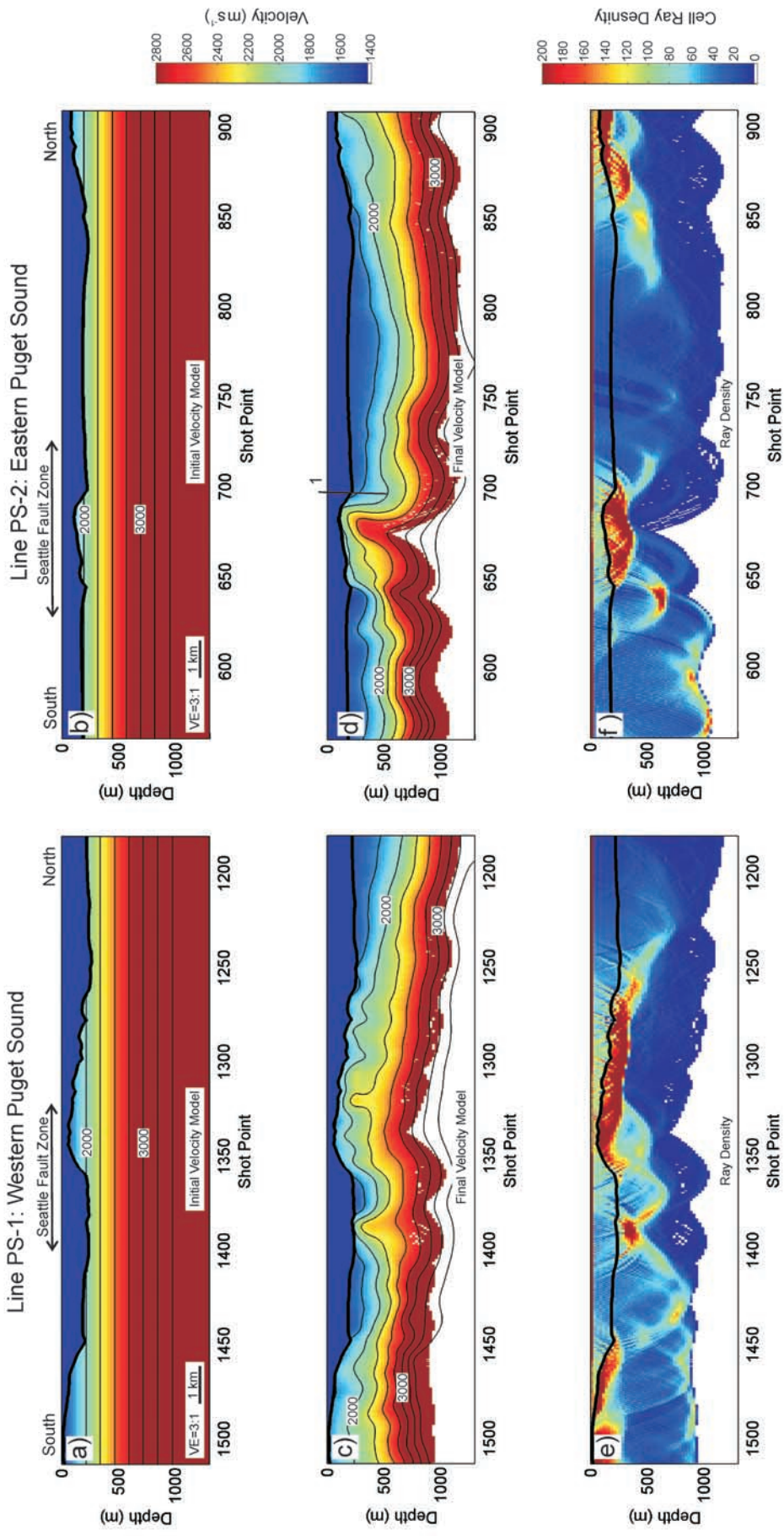

Figure 3. Tomographic inversion of first arrivals for *P* wave velocity variations across the Seattle fault zone: (a) Starting velocity model for line PS-1; (b) starting velocity model for line PS-2; (c) final velocity model for line PS-1 in western Puget Sound; (d) final velocity model for line PS-2 in eastern Puget Sound; (e) ray density in final model for PS-1; and (f) ray density in final model for PS-2. Cells of the velocity models in which no rays propagated during the final tomography iteration are shown as white. High-velocity rocks close to the seafloor indicate the position of the Seattle fault zone. The vertical line denoted by 1 indicates the north striking tear fault discussed in the text. Isovelocity contours spaced every 250 m s^{-1} are shown in Figures 3a to 3d, and the seafloor is marked by the heavy black line. The vertical exaggeration is 3:1.

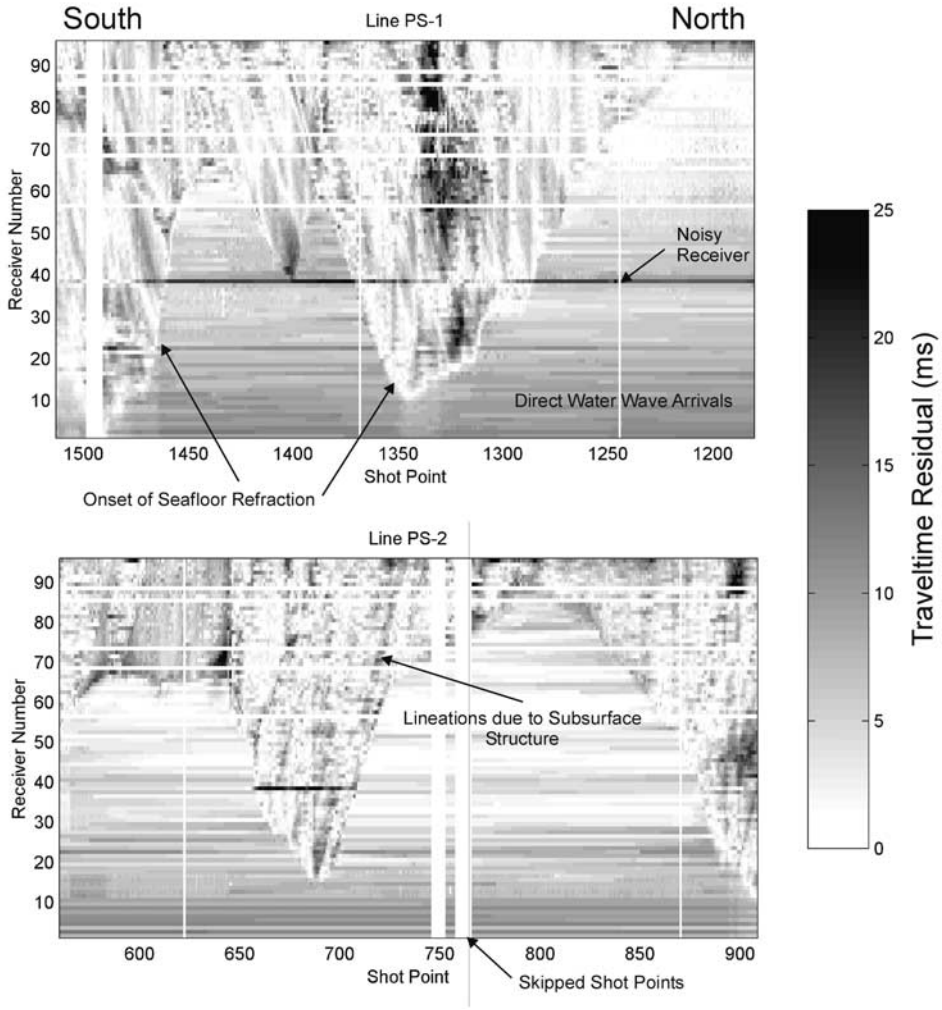

Figure 4. Plots of the travel time residuals for each shot-receiver pair for shots near the Seattle fault zone. Iterative tomographic inversion starting from an initial 1-D model reduced the RMS residual from 79 to 7 ms for line PS-1 and from 168 to 9 ms for line PS-2. Locally high travel time residuals are shown as darker areas. Vertical and horizontal bands with zero residual correspond to skipped shot points, which are shown by gaps in Figure 2, and killed receiver groups, respectively. Low receiver numbers correspond to small offsets. The crossover from the direct water wave to the seafloor refraction can usually be identified as slightly increased residual values. Diagonal bands where travel time residuals are locally elevated are probably attributable to subsurface structure.

(near SP 680 in Figure 3d). We associate these velocities with the Oligocene Blakeley Formation, which is exhumed at Alki Point 1 km east of line PS-2, because sonic logs show that most of the Blakeley Formation is characterized by velocities over 2500 m s^{-1} [*Brocher and Ruebel*, 1998]. From the strong lateral change visible in the velocity model, we infer the likely existence of a steeply dipping fault (1 in Figure 3d), along which Tertiary rocks are in contact with low-velocity Quaternary strata; this interpretation is discussed in more detail later.

[16] The velocity model along line PS-1 in western Puget Sound shows that the Seattle fault zone contains two distinct zones of uplift (SP 1385–1395 and SP 1310–1360) separated by a 1000-m-wide basin filled with up to 200 m of Quaternary sediment. The northern limit of the fault zone is less clear than on line PS-2, because the velocities of the rocks thrust close to the seafloor on PS-1 are lower, 2300 m s^{-1}, and low-velocity Holocene sediments are less prevalent. We interpret the uplifted rocks with velocities of 2300 m s^{-1} to be Miocene Blakely Harbor Formation, which exhibits lower velocities than the Oligocene Blakeley Formation and is exposed in the fault zone on Bainbridge Island, but the presence of unusually high-velocity Pleistocene rocks cannot be completely excluded. The Blakely Harbor Formation is not exposed on land near Alki Point on the east shore of Puget Sound. A short-wavelength magnetic anomaly on Bainbridge Island, which is associated with a Miocene volcanic conglomerate in the hanging wall of the Seattle fault, extends offshore to the east, and becomes somewhat less pronounced beneath eastern Puget Sound [*Blakely et al.*, 2002], consistent with our interpretation. We infer faults near the shallow high-velocity zones at SP 1330 and SP 1380, but a precise interpretation requires correlation of the

velocity model with the coincident seismic reflection sections. Shallow seismic velocities >1900 m s^{-1} occur at the seafloor between SP 1270 and SP 1360, implying that Pleistocene glacial sediments are exposed here. The undulations in the seafloor between SP 1270 and SP 1310 overlie regions of slightly elevated velocity in the Pleistocene section, as indicated by the contours in Figure 3c, and are probably associated with gentle folding of rocks in the footwall of the Seattle fault. Similar velocity variations in the Pleistocene section are not seen farther north of the Seattle fault zone.

4.2. Model Assessment

[17] Various a priori constraints on the velocity model grid, including first- and second-order derivatives, have been tested in the tomographic inversions. With reasonable constraint values, the main structure of the final velocity models does not change, but some details do vary. For example, the dip of the base of the high velocity block at SP 680 on line PS-2 can be interpreted as anywhere between 40° and 90° depending on differences in the horizontal and vertical derivative constraints used, but the unit's position along the line is unchanged. In the models presented here, only second spatial derivative, i.e., smoothness, constraints were employed, and these were chosen to be equal in vertical and horizontal directions to minimize the introduction of any directional distortion into the final models.

[18] Some parts of the final velocity models are better constrained by the travel time observations than others. Propagating rays are concentrated in the high-velocity rocks close to the seafloor, particularly in the Seattle fault zone (Figures 3e and 3f). For this reason these 200–300 m thick zones are likely well constrained by the travel times; the number of rays passing through a single 25 m by 25 m cell is usually over 200 and in places approaches 1000. In many of the deeper regions of the model, the ray density falls below 20 and the degree of constraint is more difficult to assess.

[19] The issue of lateral resolution in the final velocity model was addressed in a semiquantitative fashion by performing a corrugation test, essentially a 1-D version of the 2-D checkerboard test; the latter does not provide much useful information on vertical resolution when applied in the presence of a large vertical velocity gradient in the vertical plane. For each line, the final velocity model, with the exception of the fixed water layer, was subject to a laterally varying sinusoidal perturbation of given wavelength; the mean value of the perturbation was 10% of the slowness of the final model. Travel times were calculated for this perturbed model, and then inverted using the nonperturbed velocity values as a starting model. The degree to which these lateral velocity perturbations can be recovered provides an indication of the degree of lateral resolution in the final velocity model as a function of depth (Figure 5). The ideal result of such a test would be vertically oriented sinusoidal banding that extends uniformly across the velocity model below the seafloor.

[20] Figures 5a and 5b indicate that the corrugation with a half wavelength of 200 m is not well recovered, and this is due to the model smoothness constraints employed in the inversion, which are designed to suppress spatially localized ray path artifacts that arise from the underdetermined nature of the tomographic inversion problem. In contrast, the corrugation with a half wavelength of 400 m (Figures 5c and 5d) is well recovered to ~600 m depth south of the Seattle fault zone, but to only 400 m depth in the fault zone itself. North of the fault zone, recovery of the corrugation is poor due to the presence of a large thickness of low-velocity unconsolidated sediments in the Seattle basin, and very few subseafloor refractions arriving before the direct water wave (Figure 4). Vertical corrugations with a longer wavelength can be recovered to greater depths; for example, the corrugation with a half wavelength of 800 m can be recovered to respective depths of approximately 800 m, 500 m, and 700 m south, within, and north of the fault zone, though it should be noted that anomaly amplitudes are still not well estimated in the low-velocity Seattle basin sediments. At the south end of both lines where high velocity Crescent Formation rocks exist at around 900 m depth, a sinusoidal perturbation is recovered, but it is 180° out of phase. This pattern implies that an average layer velocity can be recovered at this depth, but that short wavelength velocity variations may be mispositioned by 800 m or so along the profile. Since such lateral velocity variations do not exist in the Crescent Formation rocks in our models, we do not consider this significant.

[21] In the context of this survey, we consider vertical resolution to be related to the correct positioning in depth of an increase in velocity, and our identification of the Crescent Formation rocks suggests that this is possible to around 900 m depth south of the Seattle fault zone. This result has been confirmed by another set of perturbation tests, in which a 10% velocity increase is added to the final model below various depths. These results are not presented since they essentially duplicate the depths obtained from the corrugation tests discussed above. In general, the various assessment tests of the final models imply that they are well resolved above the greatest depth where ray densities decrease below around 80 rays per 25 m by 25 m cell (Figures 3e and 3f). Specifically, we consider the steeply dipping velocity anomalies within the Seattle fault zone that are more than 400 m across to be well resolved.

5. Seismic Reflection Images

[22] Large lateral changes in shallow velocity, such as those identified by the tomographic inversions within the Seattle fault zone, distort the geometry of seismic reflection images and produce incorrect estimates of reflector depth. We have, however, resolved this problem by incorporating the shallow seismic velocity information into a depth migration of the coincident reflection profiles. Superimposing the velocity models derived from first arrivals on the depth migrated reflection profiles allows an integrated interpretation of these different seismic data (Figure 6).

5.1. Regional Seismic Stratigraphy

[23] A high-amplitude reflection is observed from the upper surface of the unit with velocities >3700 m s^{-1} mapped at the southern end of the seismic sections; this

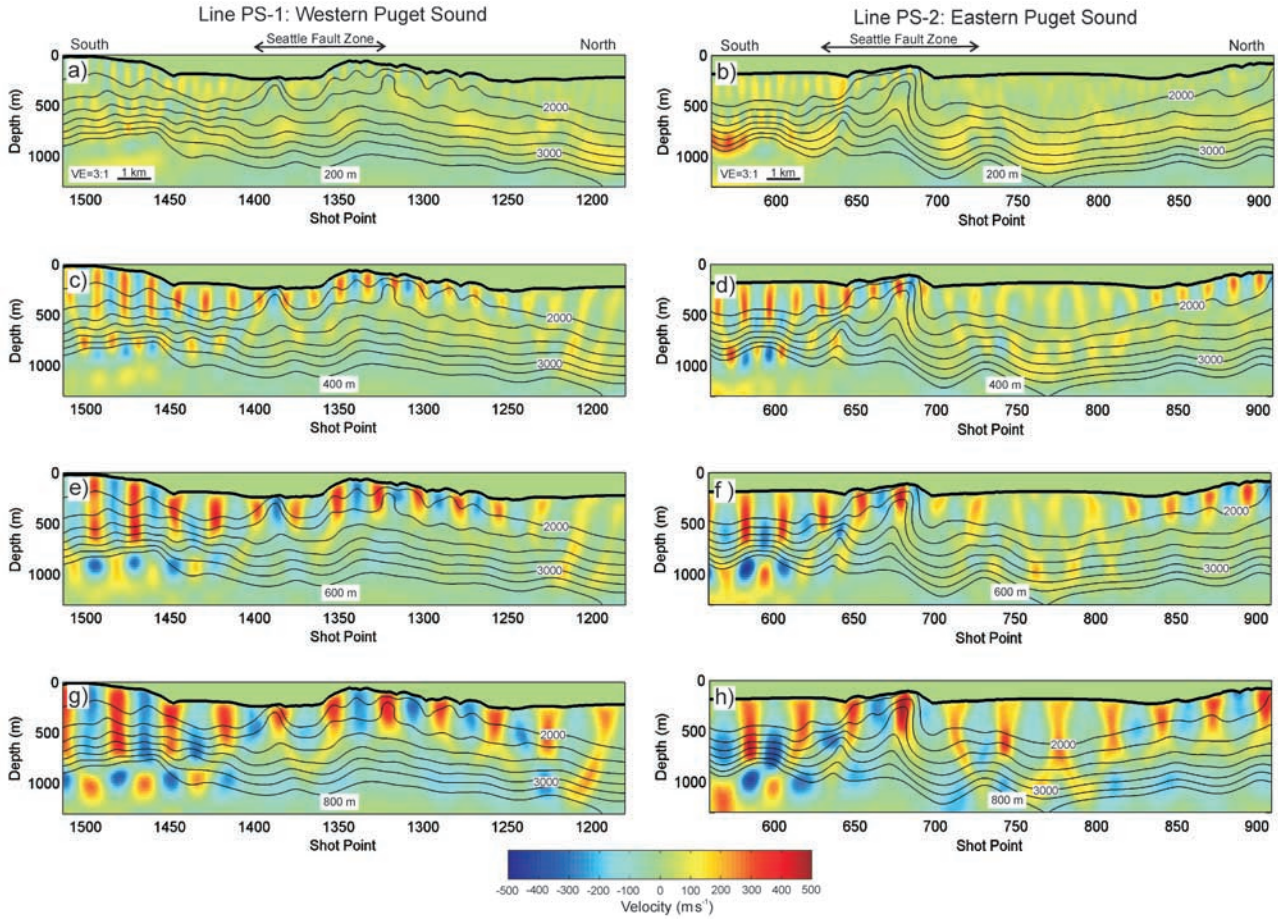

Figure 5. Assessment of final velocity models for lines PS-1 and PS-2. A vertically oriented sinusoidal perturbation with a mean value of 10% of the model slowness was added to the final velocity models below the seafloor. The depth to which sinusoidal perturbations of differing wavelengths can be recovered in these tests provides an indication of the depth of investigation and lateral resolution of the final velocity models. Artifacts associated with ray paths in the underdetermined tomographic inversion are suppressed by second derivative model smoothness constraints, which also attenuate structures with a half wavelength of 200 m or less (Figures 5a and 5b). These perturbation tests show that lateral velocity anomalies greater of 400 m can be resolved to 400 m depth within the fault zone and to 600 m depth to the south (Figures 5c and 5d). Broader velocity anomalies can be resolved to greater depths, as deep as 1000 m south of the fault zone where high-velocity Crescent Formation rocks are interpreted (Figures 5e, 5f, 5g, and 5h). The half wavelength of the imposed sinusoidal perturbation is annotated at the base of each panel. Isovelocity contours of the final velocity models spaced every 250 m s^{-1} and position of the seafloor are shown. The vertical exaggeration is 3:1.

reflection is interpreted to be the top of the volcanic rocks of the Crescent Formation (Cr in Figure 6). These rocks are folded into an anticline with the northern flank dipping at 38° on line PS-1 and 23° on line PS-2. The reflection from the top of the Crescent Formation extends down to ~1500 m depth, where it truncates against the Seattle fault zone, which is characterized by an absence of primary reflections. Crescent rocks are conformably overlain by Tertiary sediments, which truncate against an angular unconformity (U2 in Figure 6). South of the Seattle fault zone, the unconformity correlates with the 2400 m s^{-1} isovelocity contour (yellow in Figure 6). In the Seattle basin north of the fault zone, the unconformity correlates with the 2400 m s^{-1} isovelocity contour in the west but occurs near the 2500 m s^{-1} contour in the east, indicating the likely presence of high-velocity Pleistocene rocks above the unconformity. Reflections from the underlying Tertiary stratigraphy of the Seattle basin dip gently to the south, but are folded into a north dipping configuration near their truncation against the Seattle fault zone, for example, at SP 1320 on line PS-1 and SP 750 on line PS-2, probably as result of footwall deformation [*Pratt et al.*, 1997].

[24] The Quaternary section comprises two primary units separated by an unconformity (U1 in Figure 6). The lower unit, which has a chaotic appearance in the reflection sections, has velocities between 1800 and 2400 m s^{-1}, and is interpreted to be sediments of Pleistocene age [*Johnson et al.*, 1994]. The upper unit of flat-lying sedimentary strata fills small basins up to 300 m deep. The

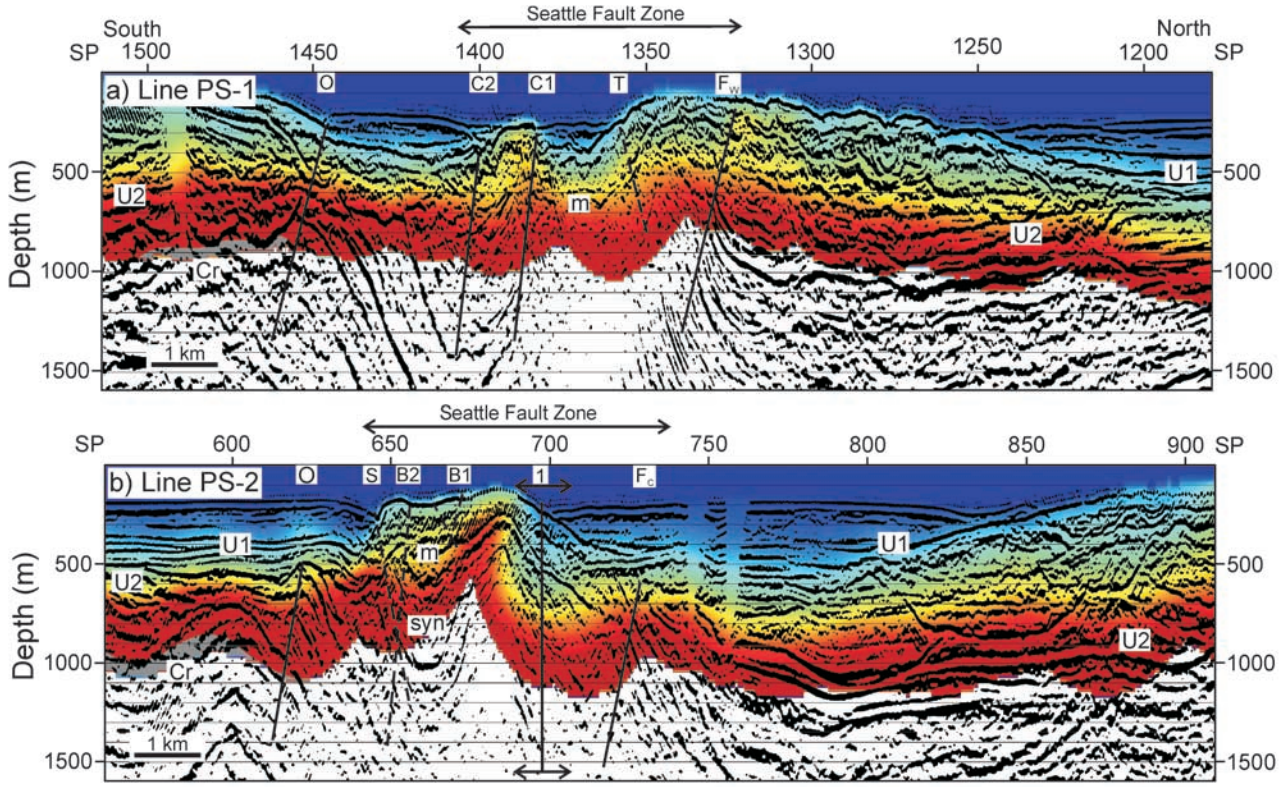

Figure 6. Superposition of velocity models on the coincident depth migrated seismic reflection sections for (a) line PS-1 and (b) line PS-2. The locations of the thrust faults identified in the velocity models are indicated by the black lines; faults whose existence is uncertain are marked with dashed lines. Low-velocity Holocene and late Pleistocene strata, which are represented by subhorizontal reflections, fill depressions in the older Quaternary sediments, which have a more chaotic character. In many areas (e.g., 1 km south of the Seattle fault zone on line PS-2) a reflection from the Tertiary-Quaternary angular unconformity is observed. At the south end of both lines, strong reflections from the top of the Crescent volcanics, which are characterized by seismic velocities >3700 m s^{-1}, occur. Colors correspond to velocity values shown in Figure 4, with the exception of gray which indicates velocities over 3700 m s^{-1}. B1, B2, C1, C2, O, S, T, and 1 identify faults discussed in the text. F_W, F_C, and F_E identify the western, central, and eastern segments of the Frontal fault. Cr, top of Crescent Formation; U1, Pleistocene-Holocene/late Pleistocene unconformity; U2, Tertiary-Quaternary unconformity; syn, syncline in folded Tertiary sediments; m, multiple. The vertical exaggeration is 3:1.

velocities of these shallow rocks are 1500–1800 m s^{-1}, implying that they are unconsolidated sediments; *Johnson et al.* [1999] have interpreted these rocks to be late Pleistocene to Holocene (postglacial) in age.

5.2. Shallow Structure of the Seattle Fault Zone

[25] On seismic reflection sections, the Seattle fault zone is generally characterized by an absence of primary reflections. Multiples and dipping coherent noise are present in the fault zone on the seismic sections displayed in Figure 6. At depth, reflections from the Tertiary and Crescent rocks cannot be followed into the fault zone, and shallow Quaternary reflections truncate against the uplifted higher-velocity Tertiary rocks. On line PS-2, the Tertiary stratigraphy is folded into a syncline within the fault zone (syn in Figure 6b) near SP 660, but the absence elsewhere of primary reflections from the Tertiary stratigraphy in the fault zone is unsurprising, because steep to overturned dips have been reported in Oligocene strata at Alki Point close to line PS-2 [*Yount and Gower*, 1991], and seismic reflection imaging of such geometries is rarely possible.

[26] Four steeply south dipping fault splays of the Seattle fault that extend close to the seafloor, denoted from north to south A, B1, B2, and C, have been previously reported in eastern Puget Sound by *Johnson et al.* [1999]. *Blakely et al.* [2002] subsequently referred to fault A as the Frontal fault, and fault C as the Orchard Point fault. We adopt this nomenclature, and will use fault F to refer to the Frontal fault and fault O to denote the Orchard Point fault. *Johnson et al.* [1999] also suggested that the Seattle fault is divided into three west striking sections that are offset by north striking discontinuous tear faults (Figure 7). As a result, they interpret the Frontal fault to be divided into three sections beneath Puget Sound, and we denote the western, central and eastern sections of the Frontal fault by F_W, F_C, and F_E, respectively. We denote the prominent tear fault beneath eastern Puget Sound that separates the central and eastern sections by fault 1. The Frontal fault is ~2.4 km

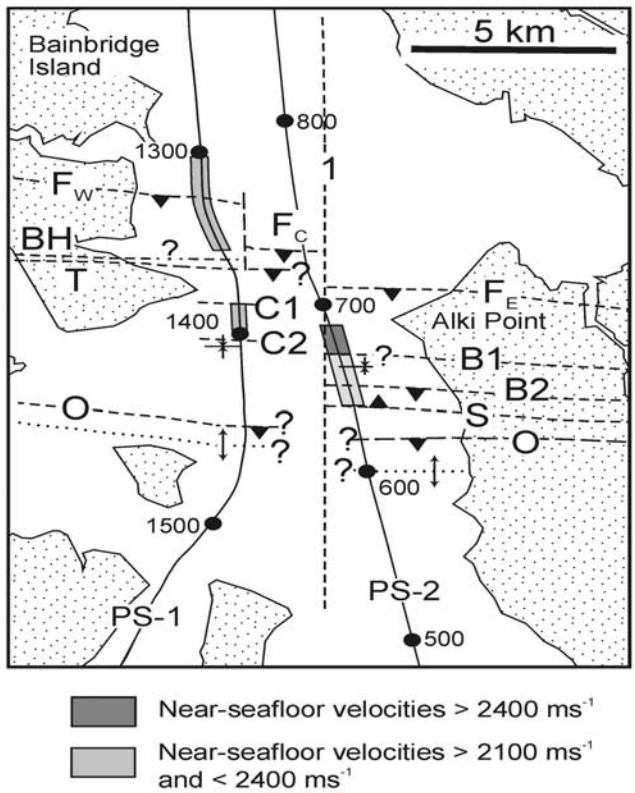

Figure 7. Detailed map modified from the interpretation of *Johnson et al.* [1999] showing sections of the Seattle fault zone beneath Puget Sound and the faults interpreted from SHIPS lines PS-1 and PS-2. Dashed lines indicate the position of interpreted faults. Dotted lines indicate fold axes. Question marks indicate positions where the existence of structures is uncertain. The position of the high-velocity rocks identified by the tomographic inversions just beneath the seafloor is shown. Letters correspond to the fault identifications of Figure 6, with BH being the Blakely Harbor fault.

farther north beneath western Puget Sound than it is in the east.

5.2.1. East Puget Sound

[27] Line PS-2 intersects the Frontal fault over the central section of the Seattle fault zone, where the top of the Tertiary is folded and apparently offset by ~100 m. The line obliquely crosses tear fault 1 at an angle of ~12° near SP 700. The dramatic lateral velocity contrast at SP 688 on line PS-2 is located 400 m south of Blakeley Formation hanging wall bedrock exposed at Alki Point, and about 1000 m south of both the northern boundary of the adjacent uplifted terrace on land and the Frontal fault imaged in this area on high-resolution seismic reflection data [*Johnson et al.*, 1999]. The velocity contrast is thus too far south to be Frontal fault splay F_E in the eastern part of the fault zone. It is similarly too far north to be fault B1, which has also been recognized onshore [*Harding et al.*, 2002]. We therefore infer that the bowl-shaped low-velocity zone within the hanging wall of the Seattle fault between SP 688 and SP 710 is associated with tear fault 1 and that the velocity contrast at SP 688 is the margin of this zone. The model assessment test and the region of high ray density suggest that the lowered velocities at 500 m depth near SP 700, i.e., the depression of the 2000 m s^{-1} velocity contour, are well constrained, but velocities could be less reliable below this level. We attribute the lowered velocities to sheared and brecciated strata of the Blakeley Formation and overlying Pleistocene unit. The extent of the low-velocity region in the east-west direction is only 250 m, but it appears broader due to the oblique crossing of fault 1 by line PS-2. If the velocity contrast at SP 688 on line PS-2 does not correspond to tear fault 1, which is our favored interpretation, then it is a previously unrecognized structure within the hanging wall of the Seattle fault, perhaps a fault or conceivably a steep fold with a strike that may not be east-west. This would imply an along-strike variation in the shallow structure of the fault zone on the scale of 1 km or less. Such variability is difficult to reconcile with current knowledge of the fault zone but cannot be completely excluded.

[28] The positions of fault splays B1 and B2 on line PS-2, as interpreted from high-resolution reflection data by *Johnson et al.* [1999], are shown in Figure 6b. Primary reflections from the syncline (syn in Figure 6b) that underlies the location of fault B1 are not offset, and we suggest that this fault either has minor offset or does not exist at this location. It should be noted that the reflection from the syncline at a depth of 1000 m yields a primary stacking velocity, but the shallower reflection at 500 m is a seafloor multiple (m in Figure 6b). Fault B2 can be interpreted as a south dipping fault that truncates the southern limb of the syncline; however, its identification is not particularly clear. Geomorphic evidence of south dipping thrusts aligned with faults B1 and B2, plus a north dipping backthrust between the eastward projections of B1 and B2, has been noted on an uplifted terrace south of Alki Point (D. J. Harding, written communication, 2002). The backthrust is not apparent in the PS-2 reflection data but could cut the northern limb of the syncline and form the south margin of the uplifted high-velocity block between SP 665 and 688. It is possible that there is another backthrust (S in Figure 6b) in the fault zone, which splays off B2 and intersects the seafloor notch at SP 640. A backthrust in this approximate location has been proposed to explain the uplift history of the Seattle fault [*ten Brink et al.*, 2002], but there is no geomorphic evidence of its existence on land [*Harding et al.*, 2002]. If backthrust *S* is present at this location, then its dip is constrained to be <30° by the presence of underlying continuous reflections observed in a nearly coincident unpublished industry seismic line.

[29] The Orchard Point fault has been interpreted within the Tertiary section 1600 m south of B2 (fault O in Figure 7) [*Johnson et al.*, 1999; *Blakely et al.*, 2002], and disruption of the uplifted terrace has been noted on land along the eastward projection of this fault [*Harding et al.*, 2002]. However, since line PS-2 shows only a minor offset of Tertiary reflections, the presence of a major fault at shallow depth in this location seems unlikely. There may be a deeper south dipping fault in the core of the anticline imaged on line PS-2 1.3 km south of splay O. The axis of the anticline corresponds to an approximately east-west oriented peak in

aeromagnetic data because volcanic rocks of the Crescent Formation are close to the surface here [*Blakely et al.*, 2002].

5.2.2. West Puget Sound

[30] We identify the western section of the Frontal fault, F_W, around 1.5 km farther north on line PS-1, than the central section, F_C intersected by line PS-2, as shown in Figure 6, which presents equivalent north-south sections. The northern limit of an uplifted terrace mapped on Bainbridge Island [*Bucknam et al.*, 1992] projects eastward into the Frontal fault, suggesting that the A.D. 900 earthquake occurred on this fault. Since this terrace does not terminate abruptly, it is likely that it was the deeper part of the Frontal fault that ruptured. Line PS-1 lies near the inferred location of a second section boundary within the Seattle fault zone; however, the existence of a north striking tear fault at this position is uncertain because high-resolution magnetic data show no offset in a prominent east-west oriented anomaly that intersects PS-1 at SP 1350 [*Blakely et al.*, 2002]. The interpretation in Figure 7 is consistent with both continuation of the prominent aeromagnetic anomaly across Puget Sound, and with the abrupt offset of the northern front of the Seattle fault zone beneath central Puget Sound.

[31] Although it might seem reasonable to interpret splay F_W of the Frontal fault on PS-1 on the north side of the higher velocity, 2300 m s^{-1} block at SP 1320, this appears inconsistent with the truncation of underlying basin reflections near SP 1330. Therefore we infer that the Frontal fault is located on the south side of this higher-velocity region, a position which is consistent with interpretations of high-resolution reflection data and onshore geological mapping. The shallow zone with velocities of 2300 m s^{-1} may represent Tertiary rocks folded upward in the footwall, or perhaps unusually high-velocity Pleistocene strata. The dip of the splay F_W of the Frontal fault is estimated to be $\sim 55°$ in the uppermost 1 km from the truncation of Seattle basin strata.

[32] Fault T in Figure 6a denotes the projection onto the seismic line of the Toe Jam Hill fault, a north dipping backthrust that has been mapped on Bainbridge Island [*Nelson et al.*, 2002]. Fault BH on Figure 7 is the Blakely Harbor fault [*Blakely et al.*, 2002] (fault B of *Johnson et al.* [1994]) and is the onland structural contact between the Eocene-Oligocene Blakeley Formation and the Miocene Blakely Harbor Formation. The absence of any reflections at this position on line PS-1 does not permit identification of the Toe Jam Hill fault or the Blakely Harbor fault. Faults C1 and C2 correspond to faults 2 and 1, respectively, of *Johnson et al.* [1994] and bound the southern block of uplifted high-velocity rocks in the fault zone. The presence of velocities around 2100 m s^{-1} at the seafloor south of fault C1 suggests that there has been at least 200 m of south side up movement along this fault. In contrast, the lack of a major velocity contrast across fault C2 implies that movement along this fault has been relatively minor; an alternative interpretation in which C2 is a small north dipping backthrust is also possible. Farther south, the Orchard Point fault appears to extend through the Crescent Formation into lower-velocity Pleistocene strata and to be aligned with a seafloor notch. The anticline just south of the Orchard Point fault correlates with the anticline interpreted on line PS-2 near SP 600 beneath eastern Puget Sound.

5.2.3. Summary

[33] Integrated tomographic and seismic reflection data thus provide significant new documentation of the Seattle fault as a broad, 5- to 7-km-wide zone of complex contractional deformation involving south dipping thrust and reverse faults, north dipping backthrusts, at least one tear fault, and tight folds. Similarly complex structural style within broad zones of contractional deformation have been described from several areas that have experienced large earthquakes, including those of the 1999 M 7.6 Chi Chi earthquake in Taiwan [*Kelson et al.*, 2001; *Lee et al.*, 2002] and the 1980 M 7.3 El Asnam earthquake in Algeria [*Philip and Meghraoui*, 1983]. Recent evidence indicates that, as with the Chi Chi and El Asnam events, several structures within the Seattle fault zone have ruptured during late Holocene earthquakes [*Nelson et al.*, 2002; *Harding et al.*, 2002]. During these earthquakes, rupture on a master fault at depth evidently propagates to the surface in a complex fashion, accommodating shortening to varying degrees along different structures. This complexity emphasizes the need for accurate identification of all significant structures within the Seattle fault zone, followed by their structural and paleoseismic characterization.

6. Segmentation of the Seattle Fault Zone

[34] The integrated interpretation of seismic reflection data and seismic velocity models shows significant along-strike differences in the number of fault splays and the degree of uplift of Tertiary rocks within the fault zone beneath Puget Sound. The most plausible interpretation of the sharp velocity contrast on line PS-2 at SP 688 is that it is associated with a north-south oriented fault that divides the Seattle fault zone into distinct segments. If this velocity contrast is not interpreted as a north-south fault, then our velocity models still demonstrate that high-velocity rocks of the Oligocene Blakeley Formation have been uplifted significantly more beneath eastern Puget Sound than in the west. There are also two distinct zones of uplift in the west, but only one in the east. These along-strike differences support the presence of a section boundary within the Seattle fault zone beneath Puget Sound, consistent with high-resolution seismic reflection data [*Johnson et al.*, 1999] and aeromagnetic data [*Blakely et al.*, 2002]. Although uplift in the A.D. 900 earthquake occurred on both sides of this boundary [*Johnson et al.*, 1999], the significant differences in the nature of the uplift we identify in our velocity models implies significant differences in fault motions shallower than 1 km depth across Puget Sound. This might be a consequence of lower magnitude earthquakes, and perhaps some $M > 7$ events, being unable to rupture a segment boundary.

7. High-Resolution Seismic Tomography of Seismogenic Crustal Fault Zones

[35] Determining the position of segment boundaries, and the depths to which they extend, is important in

assessing the seismic hazard from earthquakes with various depths of rupture initiation. Furthermore the lateral velocity variations we identify in the upper part of the Seattle fault zone, and in particular the depths of the unconsolidated Holocene basins, will likely produce significant focusing and defocusing of earthquake-generated seismic waves and consequent along-strike variations in ground motion. Unfortunately, seismic reflection surveys are unable to resolve the internal structure of much of the fault zone due to the absence of strong reflectors and interfering water layer reverberations. First arrival tomography does not suffer from these limitations, and has the ability to determine subsurface velocities to depths that are very approximately a quarter of the maximum source-receiver offset. Differences in the geometry of the contact between the high-velocity, presumably Crescent Formation, rocks of the Seattle uplift and the lower-velocity Seattle basin sediments have been successfully identified at 3–6 km depth by the crustal-scale SHIPS tomography [*Brocher et al.*, 2001], but the lateral resolution is insufficient to locate segmentation within the Seattle fault zone itself. Marine refraction profiling surveys, in which a high density of shots and long multichannel recording streamers are utilized, have the potential to determine the internal velocity structure of the fault zone to 3 km depth with a lateral resolution of a few hundred meters and could establish the significance of the various nearby geological structures mapped at the surface.

8. Conclusions

[36] The shallow velocity structure of the Seattle fault zone has been imaged by tomographic inversion of a very dense data set of first arrivals recorded in two SHIPS seismic reflection profiles shot through Puget Sound. Uplifted high-velocity rocks characterize the fault zone, but the velocity structure varies significantly along the strike of the fault zone across Puget Sound. In the east, Tertiary rocks with velocities as high as 2600 m s^{-1} are found within 170 m of the seafloor, and we interpret these to be mostly Oligocene Blakeley Formation, which is exhumed at Alki Point 1 km east of line PS-2. Line PS-2 crosses a steeply dipping, north striking tear fault, characterized by locally depressed seismic velocities, that juxtaposes high-velocity Tertiary and low velocity Holocene and late Pleistocene strata. In the west, the highest velocities in the Seattle fault zone are only 2300 m s^{-1}, and we attribute this to the likely presence of the lower-velocity Miocene Blakely Harbor Formation, which is exposed in the fault zone on Bainbridge Island, but does not crop out at Alki Point. Exposure of Miocene rocks in the hanging wall of the Seattle fault zone is attributed to the local northward propagation of the fault zone during the late Miocene or Pliocene, which trapped these rocks at the surface in the fault hanging wall. Correlative rocks in eastern Puget Sound were never uplifted and are buried in the Seattle basin. These differences in the pattern of uplift are likely attributable to the existence beneath Puget Sound of a segment boundary in the Seattle fault.

[37] **Acknowledgments.** Dave Aldridge provided considerable assistance with the modifications to the tomography inversion code. Matt Cleary expertly picked the many first arrivals. The final manuscript was improved by constructive comments from Tom Brocher and two anonymous reviewers. Funding for this project was provided by the Natural Sciences and Engineering Research Council of Canada. The field data acquisition was funded by the U.S. Geological Survey with logistical support from the Geological Survey of Canada.

References

Aldridge, D. F., and D. W. Oldenburg, Two-dimensional tomographic inversion with finite-difference traveltimes, *J. Seismic Explor.*, *2*, 257–274, 1993.

Atwater, B., and A. L. Moore, A tsunami about 1000 years ago in Puget Sound, *Science*, *258*, 1614–1616, 1992.

Blakely, R. J., R. E. Wells, C. S. Weaver, and S. Y. Johnson, Location, structure, and seismicity of the Seattle fault zone, Washington: Evidence from aeromagnetic anomalies, geologic mapping and seismic reflection data, Washington, *Bull. Geol. Soc. Am.*, *114*, 169–177, 2002.

Bourgeois, J., and S. Y. Johnson, Geologic evidence of earthquakes at the Snohomish delta, Washington, in the past 1200 years, *Bull. Geol. Soc. Am.*, *113*, 482–494, 2001.

Brocher, T. M., and A. L. Ruebel, Compilation of 29 sonic and density logs from 23 oil test wells in western Washington State, *U.S. Geol. Surv. Open File Rep., 98-249*, 41 pp., 1998.

Brocher, T. M., M. A. Fisher, and E. L. Geist, A high-resolution seismic reflection/refraction study of the Chugach-Peninsular terrane boundary, southern Alaska, *J. Geophys. Res.*, *94*, 4441–4455, 1989.

Brocher, T. M., W. J. Nokleberg, N. I. Christensen, W. J. Lutter, E. L. Geist, and M. A. Fisher, Seismic reflection/refraction mapping of faulting and regional dips in the eastern Alaskan range, *J. Geophys. Res.*, *96*, 10,233–10,249, 1991.

Brocher, T. M., T. Parsons, R. J. Blakely, N. I. Christensen, M. A. Fisher, and R. E. Wells, Upper crustal structure in Puget Lowland, Washington: Results from the 1998 Seismic Hazards Investigation in Puget Sound, *J. Geophys. Res.*, *106*, 13,541–13,564, 2001.

Bucknam, R. C., E. Hemphill-Haley, and E. B. Leopold, Abrupt uplift within the past 1700 years at southern Puget Sound, Washington state, *Am. J. Sci.*, *258*, 1611–1614, 1992.

Calvert, A. J., M. A. Fisher, and SHIPS Working Group, Imaging the Seattle fault zone with high-resolution seismic tomography, *Geophys. Res. Lett.*, *28*, 2337–2340, 2001.

Catchings, R. D., M. R. Goldman, W. H. K. Lee, M. J. Rymer, and D. J. Ponti, Faulting apparently related to the 1994 Northridge, California, earthquake and possible co-seismic origin of surface cracks in Potrero canyon, Los Angeles County, California, *Bull. Seismol. Soc. Am.*, *88*, 1379–1391, 1998.

Daneŝ, Z. F., M. M. Bonno, E. Brau, W. D. Gilham, T. F. Hoffman, D. Johansen, M. H. Jones, B. Malfait, J. Masten, and G. O. Teague, Geophysical investigations of the southern Puget Sound area, Washington, *J. Geophys. Res.*, *70*, 5573–5579, 1965.

Finn, C., W. M. Phillips, and D. J. Williams, Gravity anomaly and terrain maps of Washington, *U.S. Geol. Surv. Geophys. Invest. Map*, *GP-988*, 1991.

Fisher, M. A., et al., Seismic survey probes urban earthquake hazards in Pacific Northwest, *Eos Trans. AGU*, *80*, 13, 16–17, 1999.

Gower, H. D., J. C. Yount, and R. S. Crosson, Seismotectonic map of the Puget Sound region, Washington, *U.S. Geol. Surv. Misc. Invest. Ser. Map*, *I-1613*, 1985.

Harding, D. J., S. Y. Johnson, and R. A. Haugerud, Folding and rupture of an uplifted Holocene marine platform in the Seattle fault zone, Washington, revealed by airborne laser swath mapping, *Geol. Soc. Am. Abstr. Programs*, *34*, A-107, 2002.

Johnson, S. Y., C. J. Potter, and J. M. Armentrout, Origin and evolution of the Seattle fault and Seattle basin, Washington, *Geology*, *22*, 71–74, 1994.

Johnson, S. Y., S. V. Dadisman, J. R. Childs, and W. D. Stanley, Active tectonics of the Seattle fault and central Puget Sound, Washington-Implications for earthquake hazards, *Bull. Geol. Soc. Am.*, *111*, 1042–1053, 1999.

Kelson, K. L., K.-H. Lang, W. D. Page, C.-T. Lee, and L. C. Cluff, Representative styles of deformation along Chelungpu fault from the 1999 Chi-Chi (Taiwan) earthquake: Geomorphic characteristics and responses of man-made structures, *Bull. Seismol. Soc. Am.*, *91*, 930–952, 2001.

Khazaradze, G., A. Qamar, and H. Dragert, Tectonic deformation in western Washington from continuous GPS measurements, *Geophys. Res. Lett.*, *26*, 3153–3156, 1999.

Lee, J.-C., H.-T. Chu, J. Angelier, Y.-C. Chan, H.-C. Hu, C.-Y. Lu, and R.-J. Rau, Geometry and structure of northern surface ruptures of the 1999

M_w = 7.6 Chi-Chi Taiwan earthquake—Influence from inherited fold belt structures, *J. Struct. Geol.*, *24*, 173–192, 2002.

Ludwin, R. S., C. S. Weaver, and R. S. Crosson, Seismicity of Washington and Oregon, in The Geology of North America, vol. 1, *Neotectonics of North America*, edited by D. B. Slemmons et al., pp. 77–98, Geol. Soc. of Am., Boulder, Colo., 1991.

Mayrand, L. J., A. G. Green, and B. Milkereit, A quantitative approach to bedrock velocity resolution and precision: The LITHOPROBE Vancouver Island experiment, *J. Geophys. Res.*, *92*, 4837–4845, 1987.

Miller, M. M., D. J. Miller, C. M. Rubin, H. Dragert, K. Wang, A. Qamar, and C. Goldfinger, GPS-determination of along-strike variation in Cascadia margin kinematics: Implications for relative plate motion, subduction zone coupling, and permanent deformation, *Tectonics*, *20*, 161–176, 2001.

Nelson, A. R., S. Y. Johnson, R. E. Wells, S. K. Pezzopane, H. M. Kelsey, B. L. Sherrod, R. D. Koehler, R. C. Bucknam, R. A. Haugerud, and W. T. LaPrade, Field and laboratory data from an earthquake history study of the Toe Jam Hill fault, Bainbridge Island, Washington, *U.S. Geol. Surv. Open File Rep., 02-60*, 37 pp., 2002.

Philip, H., and M. Meghraoui, Structural analysis and interpretation of the surface deformations of the El Asnam earthquake of October 10, 1980, *Tectonics*, *2*, 17–49, 1983.

Pratt, T. L., S. Johnson, C. Potter, W. Stephenson, and C. Finn, Seismic reflection images beneath Puget Sound, western Washington State: The Puget Lowland thrust sheet hypothesis, *J. Geophys. Res.*, *102*, 27,469–27,489, 1997.

Schmid, R., T. Ryberg, L. Ratschbacher, A. Schulze, L. Franz, R. Oberhansli, and S. Dong, Crustal structure of the eastern Dabie Shan interpreted from deep reflection and shallow tomographic data, *Tectonophysics*, *333*, 347–359, 2001.

ten Brink, U. S., P. C. Molzer, M. A. Fisher, R. J. Blakely, R. C. Bucknam, T. Parsons, R. S. Crosson, and K. C. Creager, Subsurface geometry and evolution of the Seattle fault zone and the Seattle basin, Washington, *Bull. Seismol. Soc. Am.*, *92*, 1737–1753, 2002.

Wells, R. E., C. S. Weaver, and R. J. Blakely, Forearc migration in Cascadia and its neotectonic significance, *Geology*, *26*, 759–762, 1998.

Williams, R. A., W. J. Stephenson, A. D. Frankel, and J. K. Odum, Surface seismic measurements of near-surface *P*- and *S*-wave velocities at earthquake recording stations, Seattle, Washington, *Earthquake Spectra*, *15*, 565–583, 1999.

Yount, J. C., and H. D. Gower, Bedrock geologic map of the Seattle 30′ by 60′ quadrangle, Washington, *U.S. Geol. Surv. Open File Rep., 91-147*, 1991.

Yount, J. C., and M. Holmes, The Seattle fault: A possible Quaternary reverse fault beneath Seattle, Washington, *Geol. Soc. Am. Abstr. Programs*, *24*, 93, 1992.

T. M. Brocher, U.S. Geological Survey, 345 Middlefield Road, MS 977, Menlo Park, CA 94025-3591, USA. (brocher@usgs.gov)

A. J. Calvert, Department of Earth Sciences, Simon Fraser University, 8888 University Drive, Burnaby, British Columbia, Canada V5A 1S6. (acalvert@sfu.ca)

K. C. Creager and R. S. Crosson, Department of Earth and Space Sciences, University of Washington, Box 351310, Seattle, WA 98195-1310, USA. (kcc@ess.washington.edu; bob@ess.washington.edu)

M. A. Fisher, U.S. Geological Survey, 345 Middlefield Road, MS 977, Menlo Park, CA 94025, USA. (mfisher@wr.usgs.gov)

R. D. Hyndman, Pacific Geoscience Centre, Geological Survey Canada, 9860 W. Saanich Rd, P.O. Box 6000, Sidney, British Columbia, Canada V8L 4B2. (hyndman@pgc.nrcan.gc.ca)

S. Y. Johnson, U.S. Geological Survey, MS 966, Box 25046, Denver Federal Center, Denver, CO 80225, USA. (sjohnson@usgs.gov)

K. C. Miller, Department of Geological Sciences, University of Texas at El Paso, El Paso, TX 79968, USA. (miller@geo.utep.edu)

D. C. Mosher, Bedford Institute of Oceanography, Geological Survey Canada-Atlantic, 1 Challenger Dr., P.O. Box 1006, Dartmouth, Nova Scotia, Canada B2Y 4A2. (dmosher@nrcan.gc.ca)

T. E. Parsons, U.S. Geological Survey, 345 Middlefield Road, MS 999, Menlo Park, CA 94025-4702, USA. (tparsons@usgs.gov)

T. L. Pratt, U.S. Geological Survey, Department of Earth and Space Sciences, University of Washington, Box 351310, Seattle, WA 98195-1310, USA. (tpratt@usgs.gov)

G. Spence, School of Earth and Ocean Sciences, University of Victoria, Victoria, British Columbia, Canada V8W 2Y2. (gspence@uvic.ca)

U. S. Ten Brink, U.S. Geological Survey, 384 Woods Hole Road, Woods Hole, MA 02543-1541, USA. (utenbrink@usgs.gov)

A. M. Trehu, College of Oceanic and Atmospheric Sciences, Oregon State University, Oceanography Administration, Bldg. 104, Corvallis, OR 97331-8507, USA. (trehu@coas.oregonstate.edu)

C. S. Weaver, U.S. Geological Survey, Department of Earth and Space Sciences, University of Washington, Box 351310, Seattle, WA 98195-1310, USA. (craig@usgs.gov)